



# Failure Modes of Laterally Loaded Piles Under Combined Horizontal Load and Moment Considering Overburden Stress Factors

Suraparb Keawsawasvong · Boonchai Ukritchon

Received: 3 March 2019 / Accepted: 23 March 2020 / Published online: 29 March 2020  
© Springer Nature Switzerland AG 2020

**Abstract** A large number of studies on various aspects of laterally loaded piles in clay have been conducted in the literature based on experimental and numerical analyses; however, the lack of studies on the influence of the soil unit weight on the undrained capacity of the problem is obvious. In this paper, the effects of the overburden stress factors on the undrained capacity of laterally loaded piles under combined horizontal load and moment are comprehensively investigated by employing the three-dimensional (3D) finite element analysis. In the present study, soil–pile interfaces are modelled as the no-tension condition while the influences of the pile length ratios are also examined in the numerical analyses. The failure envelopes of laterally loaded

piles under combined horizontal load and moment incorporating overburden stress factors, pile length ratios are presented. Employing the normality rule to the derived failure envelopes, the failure mechanisms corresponding to the ratio between applied moment and horizontal load are postulated in this paper. An approximate solution of the failure envelope of laterally loaded piles is also proposed by using a nonlinear regression analysis, and provides a convenient tool for predicting the undrained lateral capacity of piles considering overburden stress factors in practice.

**Keywords** Finite element · Lateral pile · Combined loading · Three-dimensional · Undrained capacity

---

S. Keawsawasvong  
Department of Civil Engineering, Thammasat School of Engineering, Thammasat University, Pathumthani 12120, Thailand  
e-mail: suraparb@hotmail.com

B. Ukritchon (✉)  
Department of Civil Engineering, Centre of Excellence in Geotechnical and Geoenvironmental Engineering, Faculty of Engineering, Chulalongkorn University, Bangkok 10330, Thailand  
e-mail: boonchai.uk@gmail.com

B. Ukritchon  
Department of Civil Engineering, Center of Excellence on Earthquake Engineering and Vibration, Faculty of Engineering, Chulalongkorn University, Bangkok 10330, Thailand

## 1 Introduction

Pile foundations are conventionally considered as a general solution for supporting large structures such as offshore platforms, bridges, wind turbines, transmission towers, high-rise buildings, etc. In addition to the consideration of the vertical load-carrying capacity of piles under compressive or uplift actions, the lateral capacity of pile is another important design parameter for pile foundations under several circumstances due to wave forces, wind loadings, dynamics forces from earthquake actions, etc. In most practical cases, piles are inevitably subjected to both horizontal load and

moment induced from those different actions and forces. The prediction of the lateral capacity of piles under combined horizontal load and moment is also essential for the design of pile foundations, and hence is the subject of this paper.

A large number of studies on the analyses of laterally loaded piles have been conducted in the past. The conventional methods of analysis of the problem include limit equilibrium method (e.g., Hansen 1961; Broms 1964; Meyerhof et al. 1981; Georgiadis et al. 2013), limit analysis method (e.g., Murff and Hamilton 1993; Klar and Randolph 2008; Yu et al. 2015a, b) and finite element method (e.g., Georgiadis and Georgiadis 2010; Georgiadis 2014). The summary of the advantages and disadvantages of the existing methods of analysis can be found in Reese and Van Impe (2007) and Ruigrok (2010). It should be noted that the limit equilibrium method, the subgrade reaction method (e.g., Matlock and Reese 1960; Davisson and Gill 1963), and the  $p$ - $y$  curve (e.g., Reese 1977; Ismael 1990; Reese et al. 2000) require the solution of earth pressure distribution or lateral soil resistance under the full-flow around mechanism (e.g., Yu et al. 2015a) whose solutions are available for different shapes of piles such as circular shape (Randolph and Houlsby 1984; Martin and Randolph 2006), rectangular shape (Keawsawasvong and Ukritchon 2016a; Ukritchon and Keawsawasvong 2018) and I-shape (Keawsawasvong and Ukritchon 2017a).

At present, the finite element method (FEM) has become more popular and advanced than that in the past. This numerical method has been employed as an efficient and accurate tool to study many geotechnical problems. Some examples of the studies on foundations under combined loading (e.g., horizontal load and moment) include Ukritchon et al. (1998) for strip footings, Keawsawasvong and Ukritchon (2018) for T-shaped footings, Keawsawasvong and Ukritchon (2017b) for cantilever flood walls and Keawsawasvong and Ukritchon (2016b) for underground walls. The latter reported that there are significant differences on the undrained capacity of laterally loaded underground walls (i.e., plane strain conditions) between full-tension (no separation) or no-tension (separation) conditions. Experimental work on laterally loaded piles in clay has shown that a gap is formed between the back of the pile and the soil (Tuladhar et al. 2008).

For a practical point of view, non-dimensional design charts or closed-form equations that allow a direct computation of the undrained capacity of laterally loaded piles in clays are desirable. For example, the approach of Broms (1964) is one of conventional and classical methods for determining the ultimate lateral load of piles in clays. In his method, a set of equilibrium equations was employed along with an assumption of a simple geometrical earth pressure distribution along pile length. Hansen (1961) and Meyerhof et al. (1981) also proposed an equation of lateral pile capacity based on another assumption using different earth pressure distributions of soil reaction along pile. Nevertheless, the effect of adhesion factor at soil–pile interfaces is not taken into account in the methods by Broms (1964), Hansen (1961) and Meyerhof et al. (1981). Later, Georgiadis et al. (2013) derived analytical solutions for the undrained capacity of lateral piles near cohesive slopes by additionally considering the adhesion factor at soil–pile interfaces, the inclination of slope and the distance of pile from the crest of slope.

Weightless soil is one important assumption employed in most existing studies of the lateral pile capacity (Broms 1964; Meyerhof et al. 1981; Murff and Hamilton 1993; Klar and Randolph 2008). In addition, the effect of soil weight cannot be realistically handled in the analysis of the full-flow mechanism around pile (Randolph and Houlsby 1984; Martin and Randolph 2006; Keawsawasvong and Ukritchon 2016a, 2017a; Ukritchon and Keawsawasvong 2018) because of the assumption of the plane strain condition in the direction of the pile depth. Yu et al. (2015a, b) presented non-dimensional design charts of the lateral pile capacity in which the weight of soil was also considered. Using FEM, Zhang et al. (2016) reported that the weight of soil also contributed to the lateral pile capacity if suction was not available. So far, there are very few studies on the effect of soil weight on the lateral pile capacity in the literature, particularly for piles subjected to purely applied moment or combined horizontal load and moment.

In this paper, the effects of soil weight on the undrained lateral capacity of piles are comprehensively investigated by employing a three-dimensional finite element analysis. The present problem considers three types of lateral loading including purely applied horizontal load, purely applied moment, and combined horizontal load and moment. Soil–pile

interfaces are modelled as the no-tension condition in finite element analyses. Numerical results are presented as non-dimensional design charts that are a function of pile length ratios and overburden stress ratios accounting for the influence of soil weight combined with pile length and undrained shear strength of clays. The failure envelopes of combined horizontal load and moment of piles are developed from the numerical solutions while the associated failure mechanisms are discussed and postulated. An approximate solution of the failure envelope of laterally loaded piles under combined horizontal load and moment is proposed by normalizing it with the lateral pile capacity under purely horizontal load and pure moment. The results in this study can be applied to predict the undrained lateral capacity of piles under combined horizontal load and moment considering the effects of overburden stress factors and pile length ratios in practice.

## 2 Method of Analysis

The three-dimensional (3D) finite element analysis (FEA) with the model and computation developed through the computer software, PLAXIS3D (Brinkgreve et al. 2013) is employed to investigate the effects of overburden stress ratios and pile length ratios on the undrained lateral capacity of rigid circular piles under combined horizontal load and moment in homogeneous and isotropic clays, as shown in Fig. 1a. In the numerical investigation, the clay behavior is modelled as an elastic-perfectly plastic material obeying Tresca failure criterion in which the input parameters include undrained shear strength ( $s_u$ ), undrained Young's modulus ( $E_u = 500s_u$ ), Poisson's ratio ( $\nu = 0.495$ ), total friction angle ( $\phi = 0$ ), total dilation angle ( $\psi = 0$ ) and soil unit weight ( $\gamma$ ). The circular pile with diameter ( $D$ ) and length ( $L$ ) is assumed to behave as an elastic material, and is subjected to the combined horizontal load ( $H$ ) and moment ( $M$ ) at its top. The input parameters of the pile are Poisson's ratio ( $\nu = 0.21$ ) and Young's modulus =  $2.545 \times 10^7$  kPa, corresponding to typical properties of concrete. The interface between pile and soil is assumed to be fully rough in which the undrained shear strength at the interface is equal to that of the adjacent soil (i.e.,  $s_{ui} = s_u$ ). The soil–pile interface is modelled using the no-tension condition which allows the soil to separate

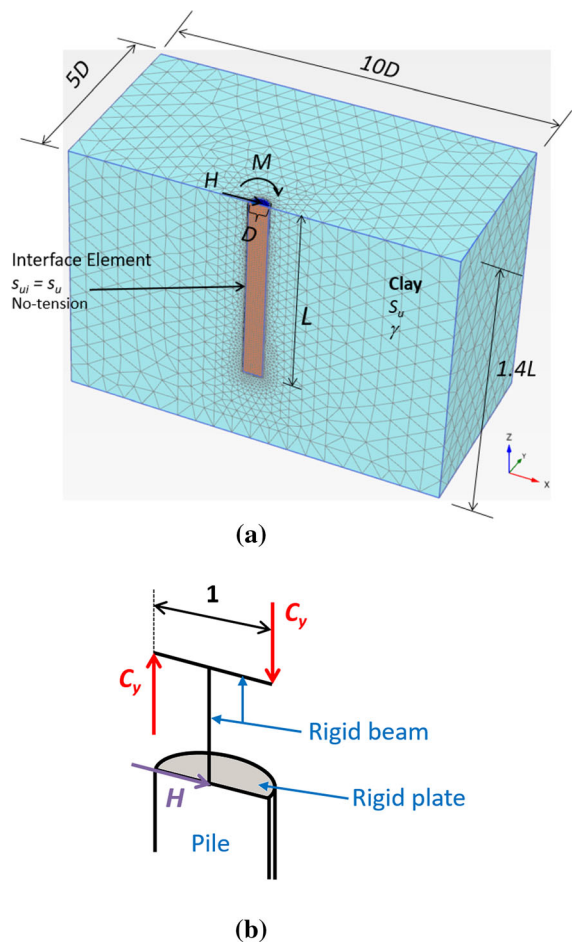


**Fig. 1** FEA model: **a** model geometry and mesh; **b** transfer mechanism of combined horizontal load and moment

from the back of the pile. This is implemented in the Tresca failure criterion using tension cut-off.

Figure 1a shows the numerical model of laterally loaded pile generated by PLAXIS3D. Since the problem of laterally loaded pile is symmetrical, only half of the model is used in FEA. A very rigid elastic pile cap modelled by a structural plate element is employed at the pile top whose center is subjected to the horizontal load ( $H$ ). This pile cap has the purpose of transferring the  $H$  load to distributed tractions on the pile top and avoiding numerical errors associated with applying the point load to the soil node. Since the moment is not allowed to be directly inputted to the structural plate element in FEA, the rigid beam elements subjected to statically equivalent couple forces ( $C_y$ ) are employed to generate the applied moment ( $M$ ), as shown in Fig. 1b.

Four types of elements were employed in the FEA model including: (1) 10-noded tetrahedral elements for the soil; (2) 6-noded triangular interface elements between the soil and the pile; (3) 6-noded triangular plate elements for the pile cap; and (4) 3-noded line elements for the moment transfer beam. It should be noted that the PLAXIS3D software allows only tetrahedral elements for soils. Thus, in the present study, it was not possible to investigate the effect of using hexahedral elements on the accuracy of the numerical solution. Readers are referred to Brinkgreve et al. (2013) for further information on element types and shape functions.

The boundary conditions for the numerical model of laterally loaded piles are set by using a typical pattern commonly used for FEA in geotechnical engineering. Zero displacements for both horizontal and vertical directions are defined at the bottom plane whereas only zero displacements for horizontal direction are defined for the vertical side planes. The top plane of soils is treated as the free surface where all directions of displacements are permitted. The sizes of boundaries are selected to be sufficiently large in order to confirm that there is no effect on the undrained lateral capacity of piles. To confirm this, the computed relative shear stress obtained from FEA is checked such that the plastic yielding zone is captured within the boundary domain, and hence implying that the size of selected domain is large enough and causes insignificant effect on the computed solutions. However, the extremely large size of the domain can result in an increase in the number of tetrahedral elements directly reducing the computational performance of numerical simulations (i.e., increasing calculation time). Based on several trial-and-error checks, the optimal sizes of the model are  $5D \times 10D \times 1.4L$  for the width, length and depth of the domain (see Fig. 1a). Figure 1a also shows a typical mesh used in FEA of the present problem. A very fine element distribution is used for discretizing piles and adjacent soils whereas a medium element distribution is used for the zone of remote soils. As a result, the sizes of elements are refined at the pile and adjacent soils, and tend to increase as they are close to the boundary of the domain.

For the proposed study, there are six dimensional parameters of laterally loaded piles, namely  $H$ ,  $M$ ,  $D$ ,  $L$ ,  $s_u$ , and  $\gamma$ . Based on the dimensionless technique

(Butterfield 1999), these six parameters can be reduced to the following dimensionless parameters as:

$$h, m = f(L/D, n) \quad (1)$$

where  $h = H/s_u LD$  is the horizontal load factor,  $m = M/s_u L^2 D$  is the moment factor,  $L/D$  is the ratio of pile length to diameter,  $n = \gamma L/s_u$  is the overburden stress factor.

The overburden stress factor  $n$  can be considered as the combined relationship between pile length ( $L$ ), the soil unit weight ( $\gamma$ ), and the undrained shear strength ( $s_u$ ). For the case of non-homogenous soil profile, the two latter can be taken as the average values of soils. Considering the practical ranges of parameters as  $\gamma = 14\text{--}20 \text{ kN/m}^3$ ,  $L = 10\text{--}100 \text{ m}$ ,  $s_u = 10\text{--}100 \text{ kPa}$ , the  $n$  factor has the range of 1.4–200. Note that the special condition of  $n = 0$  corresponds to the ideal case of weightless soils (i.e.,  $\gamma = 0$ ). The  $n$  parameter may be interpreted as the degree of the total overburden pressure of soil at pile tip as compared to its average undrained shear strength. Conversely, the reciprocal of  $n$  may be interpreted as the ratio of the average undrained shear strength of soil normalized by the total overburden pressure. Therefore, a short length pile embedded into a stiff soil gives rise to a small  $n$  ratio. In contrast, a long length pile embedded into a soft soil gives rise to a large  $n$  ratio.

It should be noted that the undrained shear strength profile ( $s_u$ ) is assumed to be constant with depth in finite element analyses. In practice, a linearly increasing undrained shear strength may be found at a site because of the effect of an increase in the effective overburden pressure in a deeper soils. However, this is beyond the scope of the present study.

### 3 Verifications with Existing Solutions

The results of the present study of piles under purely horizontal load are compared with the existing solutions from several methods such as limit equilibrium method (LEM) by Broms (1964), Meyerhof et al. (1981) and Georgiadis et al. (2013) and the upper bound (UB) limit analysis by Murff and Hamilton (1993) and Yu et al. (2015a). Note that these solutions correspond to the cases of no-tension interfaces and  $n = \gamma L/s_u = 0$  (i.e., weightless soils) except the solution of Yu et al. (2015a) who considered the effect of soil unit weight ( $\gamma \neq 0$ ). Details of each method are

**Table 1** Summary of the existing methods for the prediction of the undrained lateral capacity of piles under purely horizontal load

Existing method	Equations or design charts
Broms (1964)	$\frac{H}{s_u D^2} = -\frac{27}{2} - \frac{9L}{D} + \frac{9}{2} \sqrt{18 + \frac{8L^2}{D^2}}$
Meyerhof et al. (1981)	$\frac{H}{s_u LD} = 2F_C s_C$ , where $F_C$ = lateral resistance factor and $s_C$ = shape factor (see Meyerhof et al. 1981)
Georgiadis et al. (2013)	$\frac{H}{s_u D^2} = N_{pu} \left( 2 \frac{z_o}{D} - \frac{L}{D} \right) + \left( \frac{N_{pu} - N_{p0}}{\lambda} \right)$ , where $z_o$ can be computed from the equation below: $\omega_1 \left( \frac{z_o}{D} \right)^2 + \omega_2 \exp(-\lambda \frac{z_o}{D}) + \omega_2 \left( \frac{z_o}{D} \right) \exp(-\lambda \frac{z_o}{D}) + \omega_3 = 0$ in which $\lambda = 0.55 - 0.15\alpha$ , $\omega_1 = N_{pu}$ , $\omega_2 = 2 \left( \frac{N_{pu} - N_{p0}}{\lambda} \right)$ , $\omega_3 = -N_{pu} \left( \frac{L^2}{2D^2} \right) - \frac{N_{pu} - N_{p0}}{\lambda} \left[ \frac{1}{\lambda} + \left( \frac{L}{D} + \frac{1}{\lambda} \right) \exp(-\lambda \frac{L}{D}) \right]$ , $N_{p0} = 2 + 1.5a$ and $N_{pu} = \pi + 2 \arcsin a + 2 \cos(\arcsin a) + 4 \left[ \cos\left(\frac{\arcsin a}{2}\right) + \sin\left(\frac{\arcsin a}{2}\right) \right]$
Murff and Hamilton (1993)	$\frac{H}{s_u LD} = f\left(\frac{L}{D}\right)$ from a design chart
Yu et al. (2015a)	$\frac{H}{s_u D^2} = f\left(\frac{s_u}{\gamma D}, \frac{L}{D}\right)$ from a design chart

summarized in Table 1. Figure 2a, b show the comparisons of  $H/s_u LD$  between the present study and the existing solutions for  $n = 0$  and  $n > 0$ , respectively. As expected, all solutions indicate that an increase in  $L/D$  results in a rise of  $H/s_u LD$ . For the case of  $n = 0$  (see Fig. 2a), the UB solutions by Yu et al. (2015a) and Murff and Hamilton (1993) are significantly higher than the present study using FEA, where the former is almost three times of the present study. On the other hand, the classic LEM solutions by Broms (1964) and Meyerhof et al. (1981) are relatively smaller than the present study. The LEM solutions by Georgiadis et al. (2013) agree well with the present study using FEA when  $L/D$  is more than 10. The effect of the overburden stress factor ( $n$ ) is clearly observed in Fig. 2b in which an increase in  $n$  gives rise to an increase in  $H/s_u LD$ . For the cases of  $n > 0$ , only the solution of Yu et al. (2015a) is available for the comparison, where two  $n$  ratios of 5 and 20 are selected. Like the case of  $n = 0$ , it can be seen that the UB solutions of Yu et al. (2015a) are significantly high as compared to the present study.

#### 4 Results of Lateral Piles Under Purely Horizontal Load and Pure Moment

This section presents the extensive parametric studies of the effect of the overburden stress factor ( $n$ ) on the

undrained lateral capacity of piles under pure  $H$  or pure  $M$ . Figures 3 and 4 respectively shows the normalized load–displacement curves of purely horizontal load factors ( $H/s_u LD$ ) and pure moment factors ( $M/s_u L^2 D$ ) versus normalized displacement ( $y/D$ ), where  $y$  corresponds to the horizontal displacement at the center point on top of the pile. In the figures, the selected cases correspond to the laterally loaded pile with  $L/D = 40$ . It is evident from Figs. 3 and 4 that all curves converge to a certain value for a very large displacement, and hence the limit state condition is successfully simulated in FEA. The load–displacement curve of a high value of  $n$  converges to the limit state faster than that of a low value of  $n$ .

It should be noted that all computed numerical results including Figs. 3 and 4 are obtained by employing the arc-length control in elasto-plastic finite element analyses using PLAXIS3D. This procedure allows the numerical simulations to the limit state to be performed reliably under load-controlled calculations. As a result, the convergence of normalized load–displacement curves can be simulated accurately as shown in Figs. 3 and 4. For further details of the arc-length control procedure, refer to Brinkgreve et al. (2013).

The solutions of the present study for laterally loaded piles under purely horizontal load and pure moment are shown in Figs. 5 and 6, respectively. Clearly, it can be observed that the undrained lateral

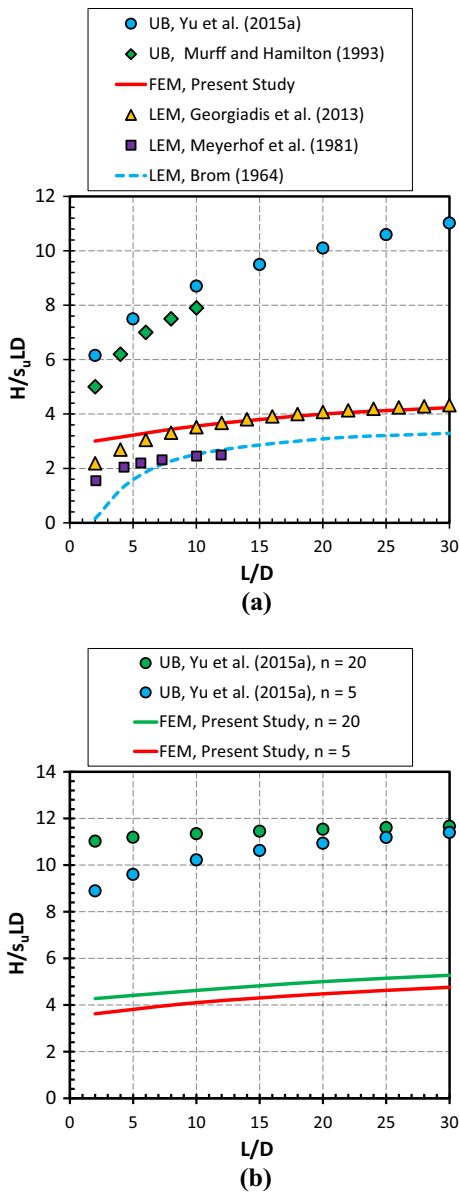


**Fig. 2** Undrained lateral capacity of piles under purely horizontal load: **a**  $n = 0$ ; **b**  $n = 5$  and  $20$

capacity of piles depends significantly on both  $L/D$  and  $n$ . In general, an increase of  $n$  or  $L/D$  results on an increase of  $H/s_u LD$  or  $M/s_u L^2 D$ . The lowest undrained lateral capacity of pile corresponds to the cases of  $n = 0$ .

Table 2 shows the study of mesh refinement on the computed numerical solutions of undrained lateral capacity of piles under purely horizontal load. In this study, the piles with  $L/D = 10$  and  $20$ , and  $n = 10$  are selected while the five levels of mesh refinement are

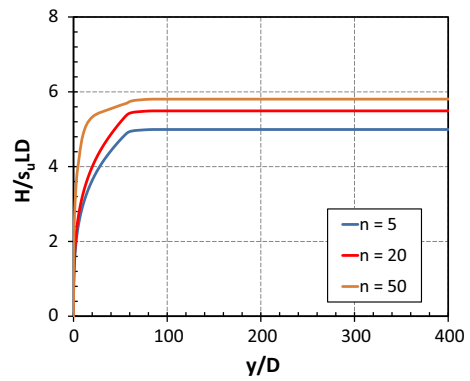


**Fig. 3** Load–displacement curves of purely horizontal load with  $L/D = 40$

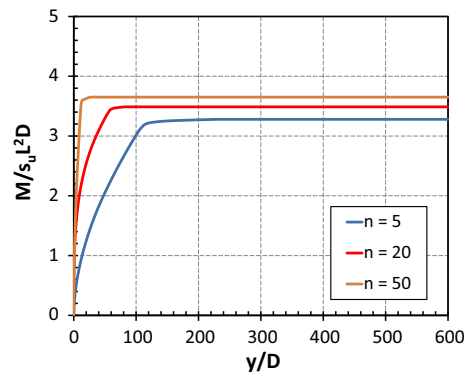


**Fig. 4** Load–displacement curves of pure moment with  $L/D = 40$

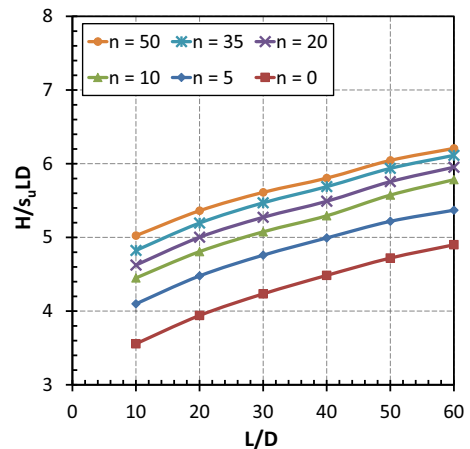


**Fig. 5** Undrained lateral capacity of piles under purely horizontal load

employed, namely very coarse, coarse, medium, fine, and very fine. The numbers of tetrahedral elements in each mesh refinement are automatically produced by



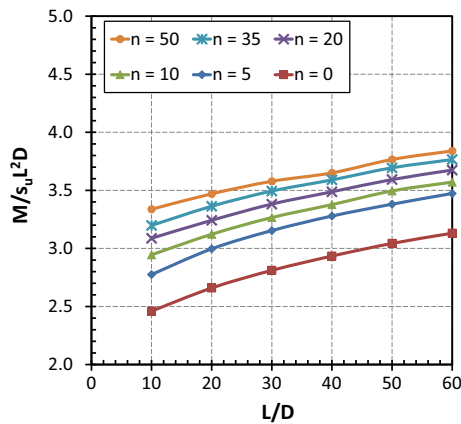


**Fig. 6** Undrained lateral capacity of piles under pure moment

PLAXIS3D using a pre-defined relative element size factor (see Brinkgreve et al. 2013). Basically, the exact number of elements mainly depend on that factor, the shape of problem’s geometry as well as boundary size. In the present study, the medium element distribution is employed in the FEA simulations because this setting requires a suitable computational time, i.e., about 6–8 h per run. It should be noted that the very fine element distribution is not practical as an extremely excessive computational time takes place, i.e., 36–48 h per run. In general, it can be observed that as the numbers of elements increase, the computed solutions tend to reduce and approach the approximate limit load from the above side. For the selected cases in Table 2, the differences of the computed solutions between the medium and very fine element distributions are very small about 1.5%, which confirms that

the selected medium refined mesh provides the right balance between accuracy and computational time.

Figure 7 shows the comparison of the incremental total displacement for laterally loaded piles with  $L/D = 40$  under purely horizontal load or pure moment for two values of the overburden stress factors  $n = 5$  and  $n = 50$ . The contour bar in the figure indicates the percentage of incremental total displacement at any point in the domain with respect to the maximum value. Thus, it represents the relative incremental total displacement varying from 0 to 100% in the domain. The rotation points of the cases of purely horizontal load and pure moment happen about  $0.75L$  and  $0.55L$ , respectively. Note that the separation between pile and soil occurs in the back side of pile (i.e., the left side) since both the horizontal load and moment overturn pile to the front side (i.e., the right side). The separation between soil and pile is found above the rotation point for both cases with  $n = 5$  and  $50$ . Thus, it can be deduced from those results that the separation distance between the back of the pile significantly depends of the overburden stress factor  $n$ . Figure 8 illustrates the failure zone of the corresponding laterally loaded piles in Fig. 7 in which the failure zone is indicated by plotting the development of plastic points. Note that the plastic point is displayed when it is located on the Tresca failure surface. It is found that the size of failure zone of laterally loaded piles increases with a decrease in the value of  $n$ . For both cases with  $n = 5$  and  $50$ , more plastic points on the front of pile and less plastic points on the back of pile are observed.

**Table 2** Effect of mesh refinement on the undrained lateral capacity of piles under purely horizontal load

$L/D$	$n$	Element distribution	Number of elements	$H/s_u LD$
10	10	Very coarse	9087	4.878
		Coarse	17,323	4.733
		Medium	59,387 (used)	4.455
		Fine	113,453	4.375
		Very fine	171,960	4.383
20	10	Very coarse	9992	5.203
		Coarse	19,690	5.088
		Medium	47,084 (used)	4.922
		Fine	114,391	4.903
		Very fine	171,204	4.847

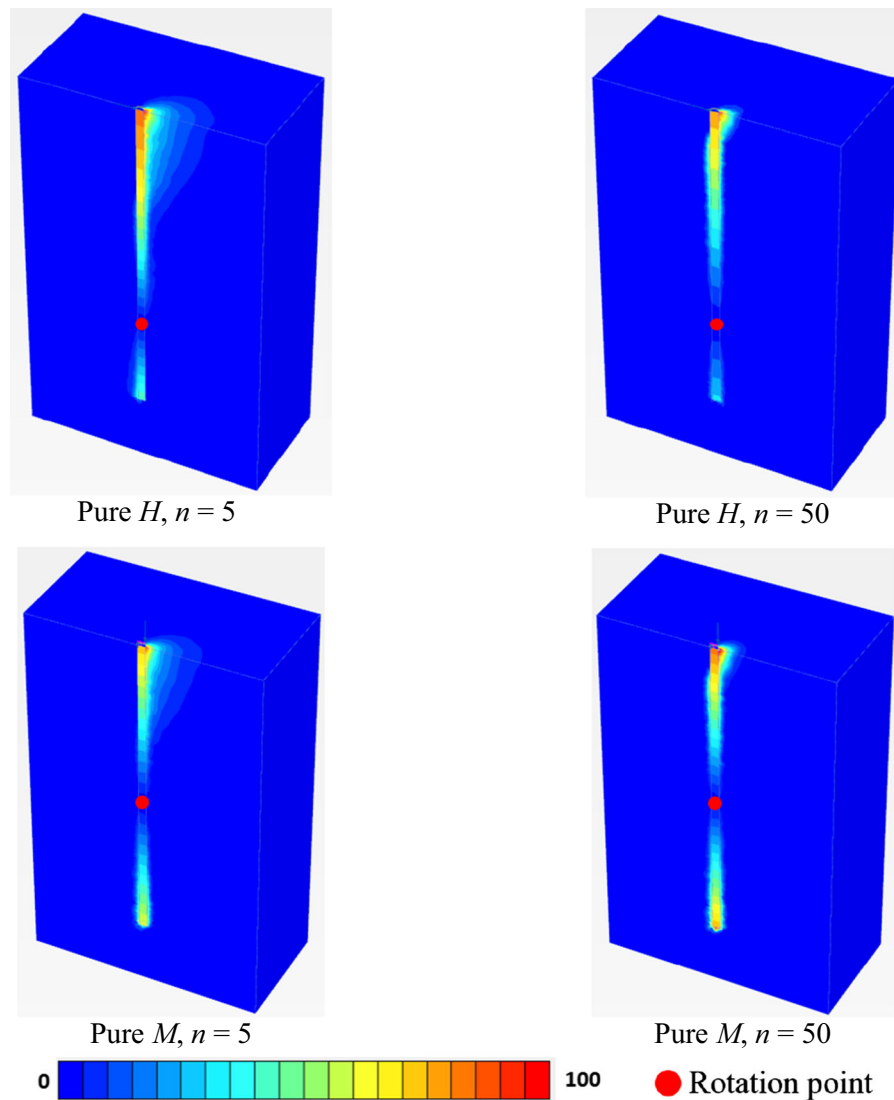


**Fig. 7** Incremental total displacements for laterally loaded piles with  $LD = 40$

## 5 Results of Lateral Piles Under Combined Horizontal Load and Moment

The failure envelopes of laterally loaded piles subjected to combined horizontal load and moment are developed as a function of the dimensionless horizontal load factor  $H/s_u LD$  and the dimensionless moment factor  $M/s_u L^2 D$ , as shown in Fig. 9. The parameter  $\beta$  is introduced and defined as the ratio between those two parameters as  $M/HL = \tan(\beta)$  or  $M = \tan(\beta)HL$ , where  $\beta$  is the angle measured from the  $+ H/s_u LD$  axis as

shown in Fig. 9a. For example, let  $\beta = 45^\circ$  and  $L = 40$  m, it can be found that the relationship between the applied moment and horizontal load is  $M = \tan(45^\circ)(40)H = kH$ , where  $k = 40$ . This loading ratio is inputted into the numerical computation of FEA. Thus, the elasto-plastic finite element calculations with the ratio of  $M = kH$  are performed until the limit state is reached in the analysis that is confirmed by the convergence of load–displacement curves as explained earlier. Figures 9b–d illustrate the failure envelopes for laterally loaded piles with three pile



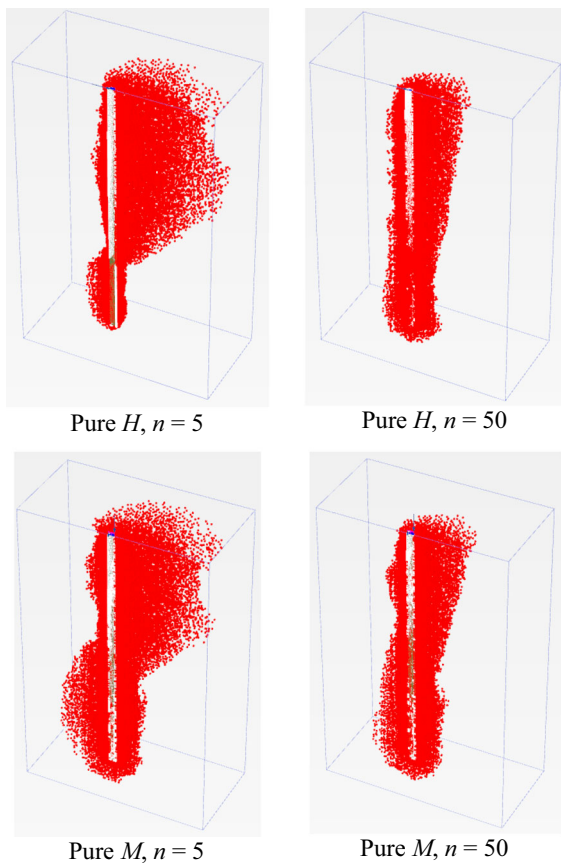


**Fig. 8** Plastic points for laterally loaded piles with  $LD = 40$

length ratios  $LD = 10, 40$  and  $60$ , respectively. For each pile length ratio, the results include two cases with  $n = 10$  and  $50$ . The failure envelopes of  $\beta = 0^\circ\text{--}90^\circ$  and  $180^\circ\text{--}270^\circ$  represent the cases where the horizontal load and moment produce overturning to the same direction. In contrast, those of  $\beta = 90^\circ\text{--}180^\circ$  and  $270^\circ\text{--}360^\circ$  represent the cases where the horizontal load and moment produce overturning to the opposite direction. Note that  $\beta = 0^\circ$  and  $90^\circ$  (or  $\beta = 180^\circ$  and  $270^\circ$ ) represent the cases of piles under purely horizontal load and pure moment, respectively. It can be observed that the failure envelope under the  $H/s_u LD\text{--}M/s_u L^2 D$  space corresponds to an ellipse whose major axis is rotated clockwise by about  $\pi/4$  measured from the positive horizontal axis. This rotated ellipse seems to be slightly distorted at the end of its semi-major axis where the convexity condition of the failure envelope still holds true. It is evident from Fig. 9b–d that the failure envelopes of the full tension cases are largest and enclose other failure

envelopes of all  $n$  values. An increase of  $n$  or  $LD$  results in an expansion of the size of failure envelopes. The observed failure envelopes constitute the major characteristics for the development of an approximate equation for predicting the capacity of laterally loaded piles under combined horizontal load and moment.

The relation of failure mechanism patterns at a point on the failure envelope is schematically illustrated in Fig. 10, and is derived using the associated flow rule (i.e., the normality rule). By this concept, a vector normal to the failure envelope represents the failure mode at the pile top, which is characterized by the incremental horizontal displacement  $\dot{\Delta}$ , and the incremental rotation  $\dot{\theta}$  corresponding to the applied  $+H$  and  $+M$ , respectively. In other words, the normal vector is the sum of each vector component of  $\dot{\Delta}$  and  $\dot{\theta}$ . The positive sign convention of  $\dot{\Delta}$  and  $\dot{\theta}$  is defined by the forward direction corresponding to the applied  $+H$  (i.e., to the right side) and  $+M$  (clockwise), respectively. For the failure envelope in the  $H\text{--}M$  space, the  $\alpha$  parameter is an angle measured from the  $+H$  axis, and is defined as  $\tan(M/H)$ . This parameter has a very strong impact on the failure mechanism of laterally loaded piles. The pattern of failure mechanism of a certain  $\alpha$  value is completely different from another. In Fig. 10, there are six important key points on the failure envelope of laterally loaded piles and the corresponding failure mechanisms can be described in Fig. 11 as follows:

*Point 1* The pile is subjected to a purely horizontal load (i.e.,  $M = 0$ ), where  $\alpha = 0^\circ$ . The rotation point of pile is located below the mid-point of pile length, where  $\dot{\Delta} > 0$  and  $\dot{\theta} > 0$

*Point 2* The pile is subjected to a purely applied moment (i.e.,  $H = 0$ ), where  $\alpha = 90^\circ$ . The rotation point of pile is located about at the mid-point of pile length, where  $\dot{\Delta} > 0$  and  $\dot{\theta} > 0$ .

*Point 3* The pile is subjected to the combined horizontal load and moment with  $H < 0$  and  $M > 0$ , where  $90^\circ < \alpha < \alpha_4$ . The rotation point of pile is located above the mid-point of pile length, where  $\dot{\Delta} > 0$  and  $\dot{\theta} > 0$ .

*Point 4* The pile is subjected to the combined horizontal load and moment with  $H < 0$  and  $M > 0$  in such a way that there is only incremental rotation at the pile top with zero incremental horizontal

**Fig. 9** Failure envelopes of laterally loaded piles under combined horizontal load and moment: **a** definition of failure envelope; **b**  $L/D = 10$ ; **c**  $L/D = 40$ ; **d**  $L/D = 60$

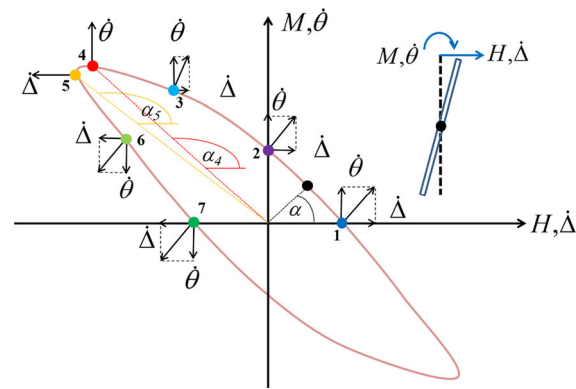
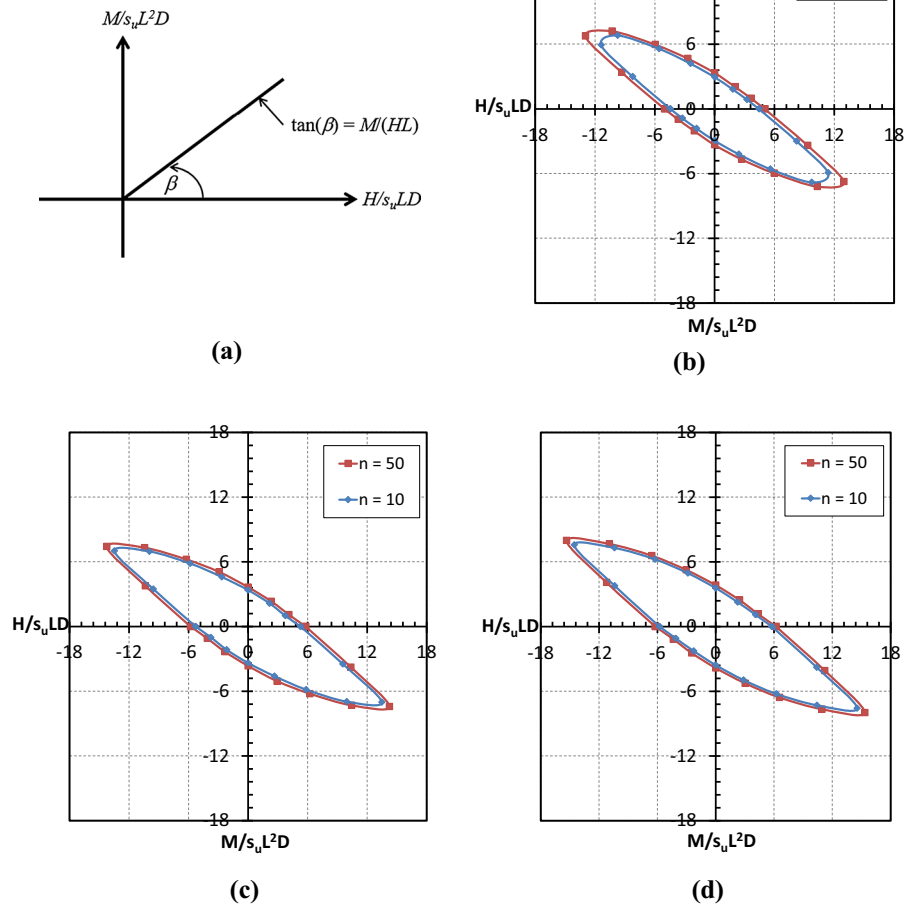


**Fig. 10** Associated flow rule applied to the failure envelope of laterally loaded piles

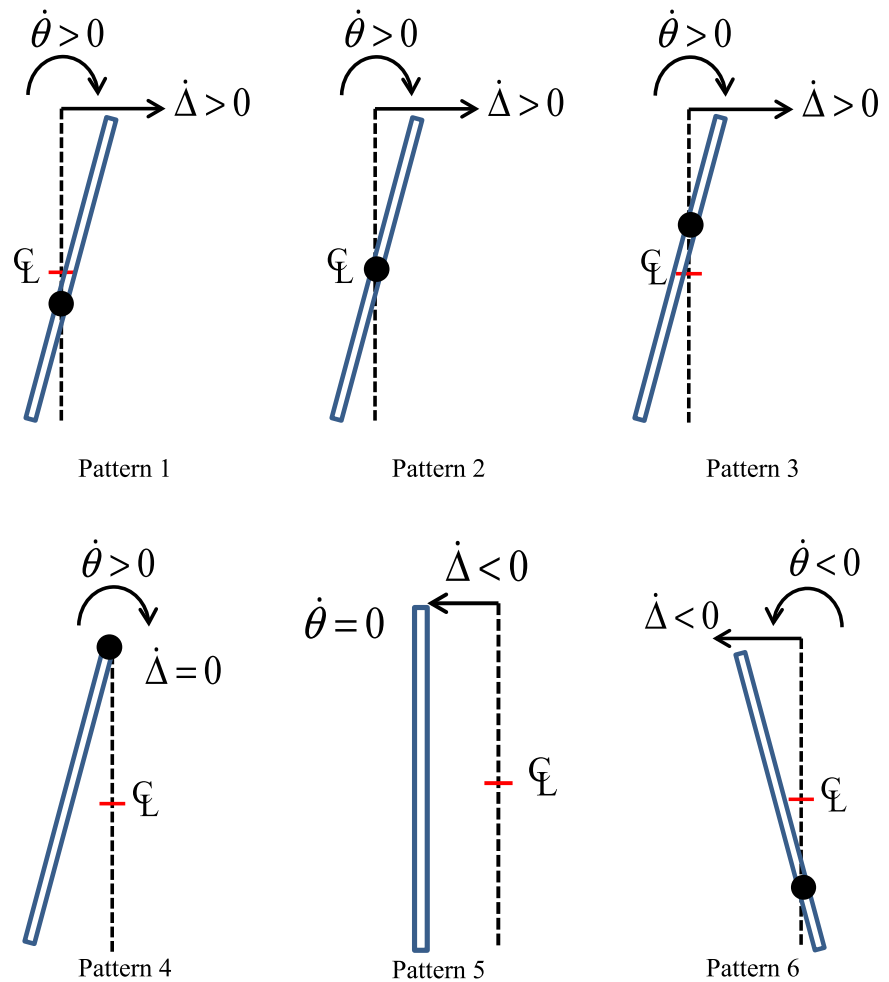
displacement, where  $\alpha = \alpha_4$  (see Fig. 10). In other words, the rotation point of pile is located at its top, where  $\dot{\theta} > 0$  and  $\dot{\Delta} = 0$ .

*Point 5* The pile is subjected to the combined horizontal load and moment with  $H < 0$  and  $M > 0$  in such a way that there is only the incremental horizontal displacement at the pile top with zero incremental rotation, where  $\alpha = \alpha_5$ . In other words, piles are undergone by pure translation to the left side, where  $\dot{\Delta} < 0$  and  $\dot{\theta} = 0$ .

*Point 6* The pile is subjected to the combined horizontal load and moment with  $H < 0$  and  $M > 0$ , where  $\alpha_5 < \alpha < 180^\circ$ . The rotation point of pile is located somewhere below the tip of pile length, where  $\dot{\Delta} < 0$  and  $\dot{\theta} < 0$ .

Note that the loading condition of Point 7 is similar to that of Point 1 except that the horizontal load is applied to the left side instead of the right side. Thus,

**Fig. 11** Failure mechanism of the points on the failure envelope



the failure mode of Point 7 is opposite to that of Point 1, and corresponds to the condition of  $\dot{\Delta} < 0$  and  $\dot{\theta} < 0$ .

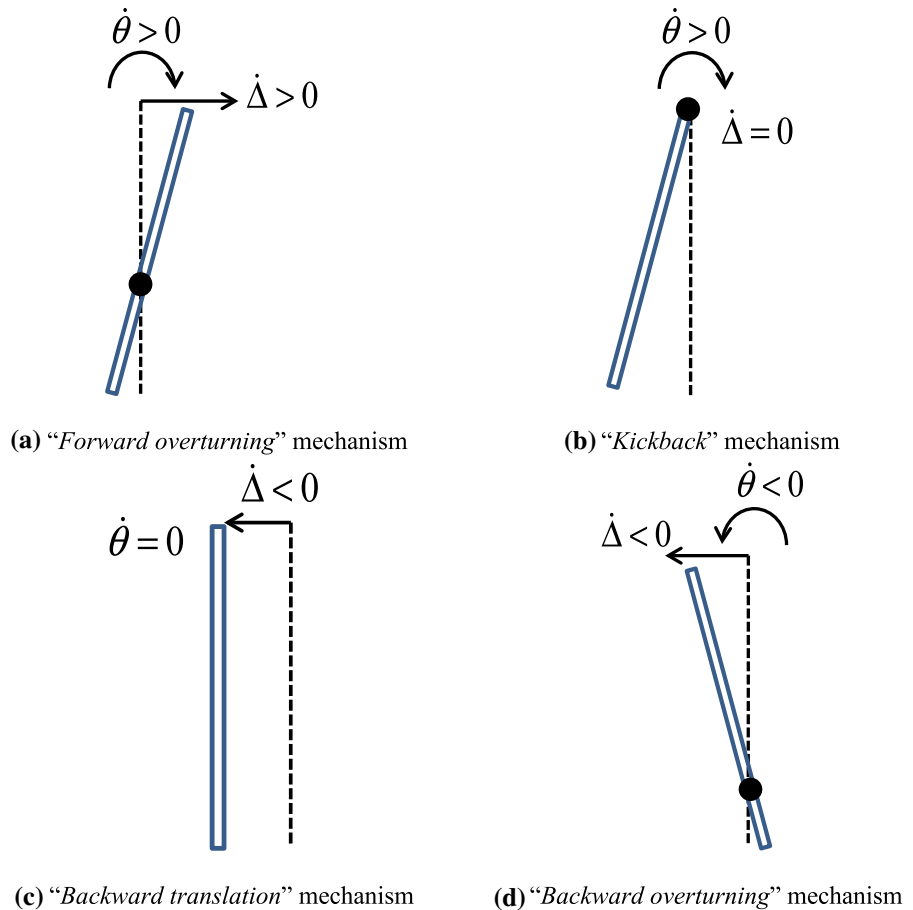
Based on the described six key points on the failure envelope, four failure modes of laterally loaded piles can be deduced in Fig. 12 as follows:

1. “Forward overturning” mechanism corresponds to the points between no. 1 and before no. 4 ( $0^\circ \leq \alpha < \alpha_4$ ) of the failure envelope, where  $\dot{\Delta} > 0$  and  $\dot{\theta} > 0$ . The pile top translates and rotates in the forward direction.
2. “Kickback” mechanism corresponds to the point no. 4 ( $\alpha = \alpha_4$ ) of the failure envelope, where  $\dot{\theta} > 0$  and  $\dot{\Delta} = 0$ . At the pile top, there is only pile rotation in the forward direction without pile translation.

3. “Backward translation” mechanism corresponds to the point no. 5 ( $\alpha = \alpha_5$ ) of the failure envelope, where  $\dot{\Delta} < 0$  and  $\dot{\theta} = 0$ . At the pile top, there is only pile translation in the backward direction without pile rotation.
4. “Backward overturning” mechanism corresponds to the points between after no. 5 and before no. 7 ( $\alpha_5 < \alpha < 180^\circ$ ) of the failure envelope, where  $\dot{\Delta} < 0$  and  $\dot{\theta} < 0$ . The pile top translates and rotates in the backward direction.

It should be noted that the failure envelope in the  $H$ – $M$  space along with parameters  $\alpha_4$  and  $\alpha_5$  depend on the dimensionless variables  $LD$  and  $n$ , and can be determined by scaling the failure envelope in the  $H/s_u LD$ – $M/s_u L^2 D$  space from employing the actual values of the problem, namely  $s_u$ ,  $L$ , and  $D$ .

**Fig. 12** Postulated failure mechanisms of laterally loaded piles under combined horizontal load



## 6 Approximate Failure Envelope

Based on the results in the preceding section, the failure envelope is quite complex as it depends on the overburden stress factor  $n$  and the pile length ratio  $L/D$ . However, a closer investigation reveals that the failure envelope can be reasonably normalized by the lateral capacity of pile under purely horizontal load and pure moment. Thus, the subscript “0” is also introduced to denote these two special cases as:  $h_0 = H_0/s_uLD$  and  $m_0 = M/s_uL^2D$ , where  $H_0 =$  purely horizontal load and  $M_0 =$  pure moment.

By employing a nonlinear regression analysis to the computed finite element solutions, the approximate expression of  $h_0$  and  $m_0$  for laterally loaded piles is proposed using the combined relationship between a power function of  $L/D$  and a rational function of  $n$  as follows:

$$h_0 = a_1 + \left( \frac{a_2n + a_3}{a_4n + 1} \right) \left( \frac{L}{D} \right) + \left( \frac{a_5n + a_6}{a_7n + 1} \right) \left( \frac{L}{D} \right)^{0.5} \quad (2)$$

where  $a_1 = 4.3671$ ,  $a_2 = 3.8909 \times 10^{-4}$ ,  $a_3 = 6.5365 \times 10^{-2}$ ,  $a_4 = 0.1056$ ,  $a_5 = 2.3647 \times 10^{-2}$ ,  $a_6 = -0.3956$  and  $a_7 = 8.1367 \times 10^{-2}$ .

$$m_0 = b_1 + \left( \frac{b_2n + b_3}{b_4n + 1} \right) \left( \frac{L}{D} \right) + \left( \frac{b_5n + b_6}{b_7n + 1} \right) \left( \frac{L}{D} \right)^{0.5} \quad (3)$$

where  $b_1 = 2.6405$ ,  $b_2 = 1.2146 \times 10^{-3}$ ,  $b_3 = 2.1488 \times 10^{-2}$ ,  $b_4 = 6.7810 \times 10^{-2}$ ,  $b_5 = 2.1137 \times 10^{-2}$ ,  $b_6 = -9.0640 \times 10^{-2}$  and  $b_7 = 6.4523 \times 10^{-2}$ .

Note that the goodness of fit of the proposed regression models in Eqs. (2) and (3) is illustrated in Figs. 13 and 14, respectively. The coefficient of determination  $R^2$  (R-squared) for  $h_0$  and  $m_0$  is 98.66% and 98.52%, respectively, which indicates reasonable

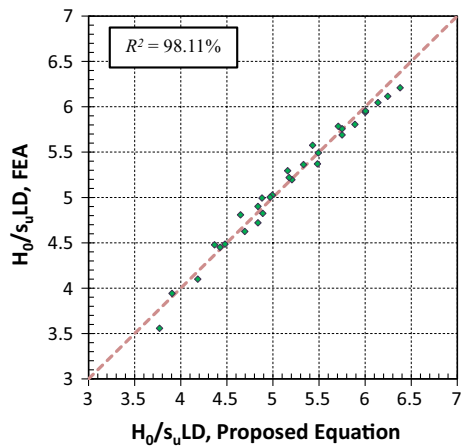


**Fig. 13** Comparison of the lateral capacity of pile under purely horizontal load between the proposed equation and the computed solution of FEA

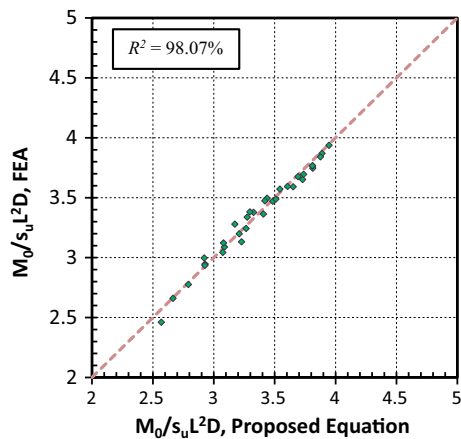


**Fig. 14** Comparison of the lateral capacity of pile under pure moment between the proposed equation and the computed finite element solutions

agreement between the predictions and the computed finite element solutions.

Finally, the normalized elliptical envelope in the  $h/h_0$ – $m/m_0$  space, which is rotated clockwise by  $\pi/4$  from the  $+h/h_0$  axis can be fitted using all data of  $L/D$  and all  $n$  values as:

$$\left(\frac{m}{m_0}\right)^2 + 1.7897mh + \left(\frac{h}{h_0}\right)^2 - 1 = 0 \tag{4}$$

Figure 15 shows the comparison of the normalized failure envelope in the  $h/h_0$ – $m/m_0$  space between the proposed regression model in Eq. (4) and the computed finite element solutions. For each case of  $L/D$  and

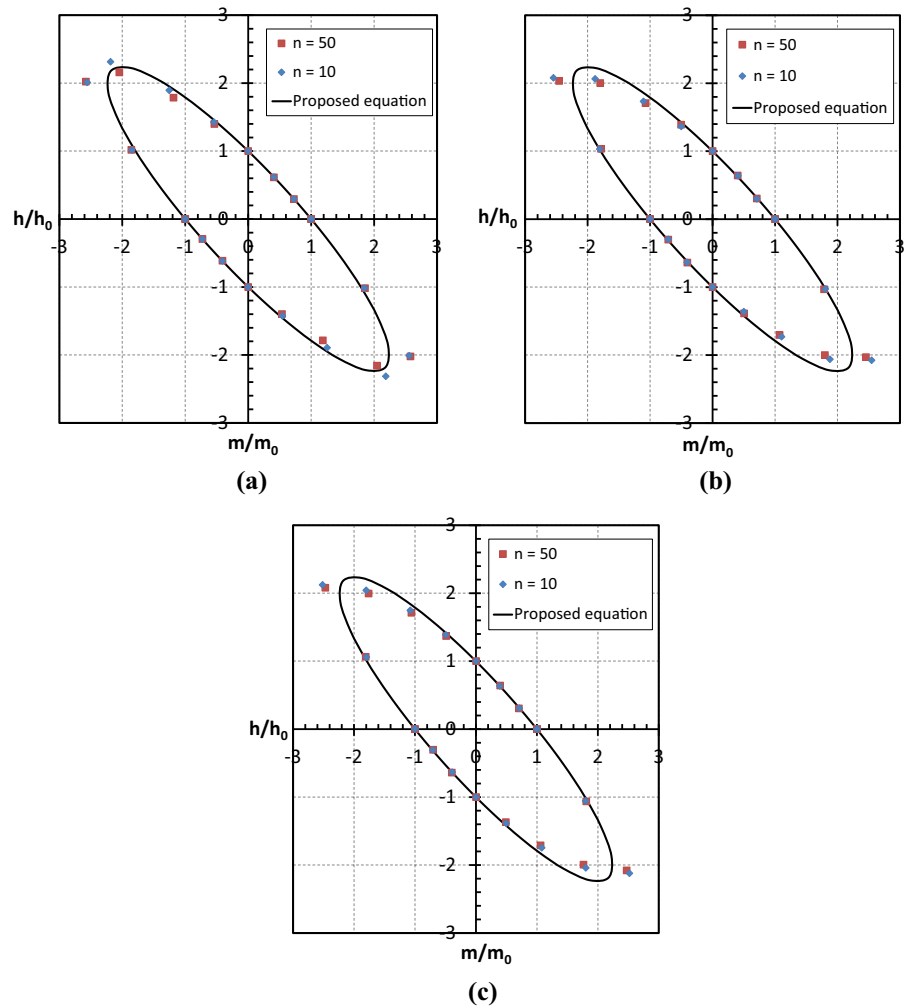
$n$ , the failure envelope is normalized with its corresponding  $h_0$  and  $m_0$ . Reasonable and good prediction between them are observed for all cases. Consequently, the failure envelope in the  $h$ – $m$  space can be scaled from  $h/h_0$  and  $m/m_0$  by employing the proposed expressions of  $h_0$  and  $m_0$  in Eqs. (2) and (3). Similarly, the failure envelope in the  $H$ – $M$  space can be obtained by multiplying  $h$  and  $m$  by the corresponding denominator (i.e.,  $s_uL$  or  $s_uL^2D$ , respectively).

### 7 Conclusions

Three-dimensional finite element analyses are employed to investigate the undrained failure modes of laterally loaded piles under combined horizontal load ( $H$ ) and moment ( $M$ ) considering overburden stress factors ( $n$ ) and pile length ratio ( $L/D$ ). The important results of the present study can be summarized as follows:

1. The combined effects of soil unit weight ( $\gamma$ ), length of pile ( $L$ ), and undrained shear strength of clays ( $s_u$ ) are represented by the overburden stress factor  $n = \gamma L/s_u$ . It is found that this parameter has the profound influence of the failure behavior of laterally loaded piles under combined horizontal load and moment.
2. For weightless soils, good agreement of the undrained capacity of piles under purely horizontal load between the present study and the limit equilibrium method by Georgiadis et al. (2013) is observed when the pile length ratio ( $L/D$ ) is greater than 10. For non-zero weight of soils, there are significant discrepancies of the undrained capacity of piles under purely horizontal load between the present study and Yu et al. (2015a).
3. The failure envelope of piles under combined horizontal load and moment in the  $H/s_uL$ – $M/s_uL^2D$  space (i.e., the  $h$ – $m$  space) is an ellipse whose major axis is rotated clockwise by about  $\pi/4$  measured from the  $+H/s_uL$  axis. There is the dependency between the size of failure envelopes and the overburden stress factor ( $n$ ) and the pile length ratio ( $L/D$ ). In particular, as the overburden stress factor increases, the elliptical rotated failure envelope expands its size. Employing the corresponding lateral pile capacity under purely horizontal load  $h_0$  and pure moment  $m_0$ , all failure

**Fig. 15** Comparison of the normalized failure envelope of pile under the combined horizontal load and moment between the proposed equation and the computed finite element solutions: **a**  $L/D = 10$ ; **b**  $L/D = 40$ ; **c**  $L/D = 60$



envelopes can be reasonably normalized under the  $h/h_0$ – $m/m_0$  space.

4. Employing the normality rule to the failure envelopes in the  $H$ – $M$  space, the failure modes of laterally loaded piles can be grouped as four mechanisms, namely forward overturning, kick-back, backward translation, and backward overturning. Each mechanism depends on the ratio of the applied moment and the applied horizontal load, and is characterized by the vector normal to the failure envelope in the  $H$ – $M$  space. The normal vector can be resolved into two components including the incremental horizontal displacement and the incremental pile rotation at the pile top.
5. In practice, the prediction of the undrained lateral capacity of laterally loaded piles under combined horizontal load and moment can be conveniently

performed using the proposed approximate expressions for the failure envelope as well as the lateral pile capacity under purely horizontal load and pure moment. The effects of overburden stress factors as well as pile length ratios are well incorporated into the proposed expression.

6. Since the results of the present study are based solely on finite element analyses, further verification of the presented results via experimental testing is required.

## References

- Brinkgreve RBJ, Engin E, Swolfs WM (2013) PLAXIS3D 2013, The Netherlands



- Broms BB (1964) Lateral resistance of piles in cohesive soils. *J Soil Mech Found* 90(2):27–63
- Butterfield R (1999) Dimensional analysis for geotechnical engineering. *Géotechnique* 49(2):357–366
- Davissom MT, Gill HL (1963) Laterally loaded piles in a layered soil. *J Soil Mech Found* 89(3):63–94
- Georgiadis K (2014) Variation of limiting lateral soil pressure with depth for pile rows in clay. *Comput Geotech* 62:164–174
- Georgiadis K, Georgiadis M (2010) Undrained lateral pile response in sloping ground. *J Geotech Geoenviron Eng* 136(11):1489–1500
- Georgiadis K, Georgiadis M, Anagnostopoulos C (2013) Lateral bearing capacity of rigid piles near clay slopes. *Soils Found* 53(1):144–154
- Hansen BJ (1961) The ultimate resistance of rigid piles against transversal forces. *Dan Geotech Inst Bull* 12:5–16
- Ismael NF (1990) Behavior of laterally loaded bored piles in cemented sands. *J Geotech Geoenviron Eng* 116(11):1678–1699
- Keawsawasvong S, Ukritchon B (2016a) Ultimate lateral capacity of two dimensional plane strain rectangular pile in clay. *Geomech Eng* 11(2):235–251
- Keawsawasvong S, Ukritchon B (2016b) Undrained capacity of laterally loaded underground walls subjected to horizontal load and moment. *J GeoEng* 11(2):75–83
- Keawsawasvong S, Ukritchon B (2017a) Undrained lateral capacity of I-shaped concrete piles. *Songklanakarin J Sci Technol* 39(6):751–758
- Keawsawasvong S, Ukritchon B (2017b) Finite element analysis of undrained stability of cantilever flood walls. *Int J Geotech Eng* 11(4):355–367
- Keawsawasvong S, Ukritchon B (2018) Three-dimensional interaction diagram for the undrained capacity of inverted T-shape strip footings under general loading. *Int J Geotech Eng* 12(2):133–146
- Klar A, Randolph MF (2008) Upper-bound and load-displacement solution for laterally loaded piles in clays based on energy minimization. *Géotechnique* 58(10):815–820
- Martin C, Randolph MF (2006) Upper-bound analysis of lateral pile capacity in cohesive soil. *Géotechnique* 56(2):141–145
- Matlock H, Reese LC (1960) Generalized solutions for laterally loaded piles. *J Soil Mech Found* 86:63–91
- Meyerhof GG, Mathur SK, Valsangkar AJ (1981) Lateral resistance and deflection of rigid walls and piles in layered soils. *Can Geotech J* 18(1):159–170
- Murff JD, Hamilton JM (1993) P-ultimate for undrained analysis of laterally loaded piles. *J Geotech Geoenviron Eng* 119(1):91–107
- Randolph MF, Houlsby GT (1984) The limiting pressure on a circular pile loaded laterally in cohesive soil. *Géotechnique* 34(4):613–623
- Reese LC (1977) Laterally loaded piles: Program documentation. *J Geotech Geoenviron Eng* 103(4):287–305
- Reese LC, Van Impe WF (2007) *Single piles and pile groups under lateral loading*. Taylor & Francis Group plc, London
- Reese LC, Wang ST, Isenhower WM, Arrellaga JA (2000) *Computer program LPILE plus Version 4.0 technical manual*. Ensoft, Inc., Austin, TX
- Ruigrok JAT (2010) *Laterally loaded piles models and measurements*. Ph.D. thesis, Delft University of Technology, The Netherlands.
- Tuladhar R, Maki T, Mutsuyoshi H (2008) Cyclic behavior of laterally loaded concrete piles embedded into cohesive soil. *Earthq Eng Struct Dyn* 37:43–59
- Ukritchon B, Keawsawasvong S (2018) Undrained lateral capacity of rectangular piles under a general loading direction and full flow mechanism. *KSCE J Civ Eng* 22(7):2256–2265
- Ukritchon B, Whittle AJ, Sloan SW (1998) Undrained limit analysis for combined loading of strip footings on clay. *J Geotech Geoenviron Eng* 124(1):265–276
- Yu J, Huang M, Zhang C (2015a) Three-dimensional upper-bound analysis for ultimate bearing capacity of laterally loaded rigid pile in undrained clay. *Can Geotech J* 52(11):1775–1790
- Yu J, Huang M, Zhang C (2015b) Ultimate lateral resistance of laterally loaded piles in undrained clay. In: Meyer V (ed) *3rd international symposium on frontiers in offshore geotechnics (ISFOG)*. Taylor & Francis Group, Oslo, Norway, pp 661–666
- Zhang Y, Andersen KH, Tedesco G (2016) Ultimate bearing capacity of laterally loaded piles in clay—some practical considerations. *Mar Struct* 50:260–275

**Publisher's Note** Springer Nature remains neutral with regard to jurisdictional claims in published maps and institutional affiliations.